NUMERICAL CHARACTERIZATION OF MATERIAL ELASTIC PROPERTIES FOR RANDOM FIBER COMPOSITES

Lucian Iorga, Yi Pan and Assimina Pelegri

NUMERICAL CHARACTERIZATION OF MATERIAL ELASTIC PROPERTIES FOR RANDOM FIBER COMPOSITES

Lucian Iorga, Yi Pan and Assimina Pelegri

This paper presents a numerical investigation of the material elastic properties for short-length mostly in-plane random fiber composites, based on microscale geometrical modeling. The particular case considered is that of materials in which the majority of fibers' orientations are contained or slightly deviate from a dominant plane. Representative volume elements for two types of random fiber composite material geometries with different fiber aspect ratios and volume fractions are generated using a novel technique. The elastic properties of the equivalent homogeneous material are determined using direct three-dimensional finite element analysis. A windowing-type analysis is employed to investigate the influence of the fiber distribution homogeneity on the homogenized elastic properties. The results are compared and validated using two alternative approaches — first, by orientation averaging of the stiffness tensor of the equivalent unidirectional composite determined by direct FEM analysis and, second, by employing the laminated random strand method.

1. Introduction

With the maturing of the preforming technologies, random fiber composites have received increased attention in recent years as potential replacements for traditional structural materials, especially steel, given the significant weight savings they offer. Already, such materials, particularly chopped glass fiber composites, have been adopted in the automotive industry for manufacturing nonstructural components [Dahl et al. 2005], and a significant effort is under way towards the utilization of carbon reinforced random composites, which offer weight savings of 50–70% relative to steel.

The utilization of such novel materials for safety critical applications requires, first, reliable estimates of the overall material properties following a homogenization process that allows for efficient analysis of large scale structures and, second, good predictions of the microlevel properties for predefined macroscale loadings.

The traditional approach in composite continuum micromechanics analysis is to employ a mean field model which, for the case of random fiber composites can be used together with an orientation averaging procedure to account for the fiber orientation randomness. Mean field models allow the estimation of material properties based on Eshelby's field solution for single ellipsoidal inclusions in an infinite medium (matrix) [Eshelby 1957]. Despite their approximate nature, given the specific assumptions, such methods offer the advantage of analytical or semianalytical results which require only a reduced

computational effort. The extension to the family of effective field methods based on the original work by Mori and Tanaka [1973] has enjoyed substantial interest, particularly following the clarifications offered by Benveniste [1987]. The Mori–Tanaka approach is based on the fundamental assumption that within a concentrated composite with many identical inclusions, that is, fibers, each inclusion experiences a far-field strain equal to the average matrix strain. This allows the determination of the Mori–Tanaka strain concentration tensor as a function of the Eshelby's strain concentration tensor obtained for the dilute case.

A substantially different approach consists in evaluating highly resolved fields for specific micro-geometries representing the analyzed material. A volume element has to be generated and must be sufficiently large to statistically represent the material and completely characterized in the microgeometry sense. The microlevel stress and strain fields due to a macroscopic loading are resolved using numerical analysis, for example, using an FEM approach.

For the case of mostly in-plane oriented random fiber composites, only relatively few studies based on direct numerical analysis can be documented in the literature [Gusev et al. 2002; Duschlbauer et al. 2006]. In this study we propose to investigate the elastic properties of two composite materials consisting of an epoxy matrix reinforced by short glass fibers. First, we investigate the corresponding representative volume elements via a homogenization scheme based on the direct three-dimensional FEM solution of the stress and strain fields. Second, we investigate the material homogeneity for relatively large structures, meaning at the macroscopic scale, in order to evaluate the applicability of the representative volume element (RVE) based homogenized model.

2. Microscale geometry generation

The microscale geometry generation algorithm used in this work is essentially a random sequential adsorption (RSA) technique, widely used in the literature for studies of particle reinforced composites. Various particle shapes have been considered for this type of geometry generation, including spherical or spherocylindrical particles [Coelho et al. 1997; Williams and Philipse 2003] or cylindrical rods [Williams and Philipse 2003; Duschlbauer et al. 2006; Kari et al. 2007; Pan et al. 2007]. The specific algorithm's application and implementation on random chopped fiber composites are described in detail elsewhere [Pan et al. 2007] and we will only briefly outline it here, for the sake of completeness.

The RSA technique for generating a RVE geometry implies iteratively adding cylinders in the pre-scribed rectangular parallelepiped volume occupied by the RVE. In the current approximation, each cylinder represents the volume occupied by one fiber bundle. The center point $C(x)$, the in-plane orientation angle ϕ, and the out-of-plane orientation angle θ (see Figure 1) of each newly generated cylinder are chosen randomly. The orientation angle selection can be done with a probability defined by a fiber orientation distribution function, $f(\phi, \theta)$. Following the definition of a new cylinder, an intersection test, based on the algorithm presented by Eberly [2001], is carried out to determine any possible intersections with the cylinders previously accepted in the configuration. No intersection between two cylinders is accepted, with the minimum distance between cylinders being set to 5% of the cylinder radius, to avoid both the generation of excessively steep stress gradients and meshing difficulties. An investigation of the influence of the minimum distance on the local stress fields is detailed in [Pan et al. 2007].
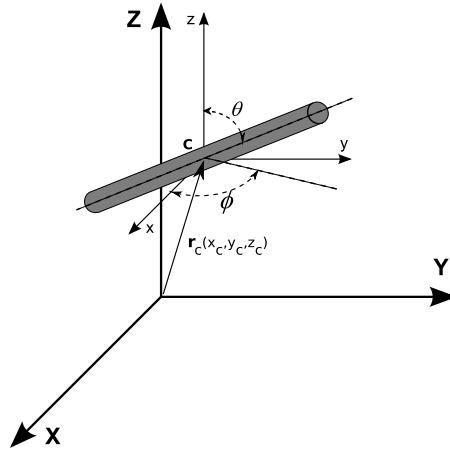
Figure 1. Fiber bundle location and orientation definition.

A provision is made in the current algorithm for the generation of periodic RVE geometries, that is, fiber arrangements that ensure material continuity across the boundaries when multiple RVEs are aggregated for the generation of a macrostructure. Specifically, when a newly generated cylinder intersects the boundaries of the RVE parallelepiped, a *clone* cylinder with the same orientation angles ϕ and θ is created on the opposite side of the parallelepiped in order to ensure geometry periodicity. This amounts to the inclusion of the volume of a full cylinder but doubles the number of intersection checks required. The flowchart of the RSA is shown in Figure 2.
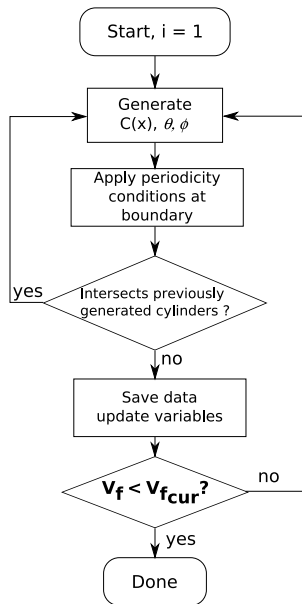

Figure 2. Random sequential adsorption flowchart.

We consider in this study two random glass-fiber material configurations and the associated micro-geometries, with predominantly in-plane fiber distributions. The configurations qualitatively represent a composite panel manufactured using the programmable powdered preform process. As such, no fiber intersections are accepted with the upper and lower parallelepiped surfaces, which correspond to the panel surfaces. However we do not account for variations in fiber length, fiber contact and fiber agglomerations observed to occur in practice, which help significantly increase the maximum achievable fiber volume fraction up to 35%–40%.

The first configuration is that of a short fiber composite with fiber aspect ratio $AR = 10$ and fiber volume fraction of $v_f = 15\%$. Geometry periodicity conditions are enforced and the out-of-plane fiber orientation angle is limited to $\pm 10°$ ($\theta \in [80°, 100°]$), while the in-plane angle ϕ is selected with uniform probability in the full-circle interval, $\phi \in [0°, 360°]$, per fabrication restrictions. The second geometry configuration considers fibers with aspect ratio $AR = 20$ and fiber volume fraction $v_f = 20\%$ but with the out-of-plane orientation angle limited to $\pm 5°$ ($\theta \in [85°, 95°]$), while uniform probability in-plane orientation is maintained.

The RVEs generated using the RSA technique will be named, for the remainder of the paper, RVE1 and RVE2, for the first ($v_f = 15\%$) and the second ($v_f = 20\%$) configuration respectively. They are defined using 124 and 227 cylinders, respectively, contained in cuboids of dimensions $3.00 \times 3.00 \times 0.60$ and $2.00 \times 2.00 \times 0.40$, where the dimensions are normalized to the fiber length. The cylinder arrangements are shown in Figure 3.

The statistics of the fiber orientation for the two RVEs are presented in terms of the probability density distribution of the orientation angles ϕ and θ. Figure 4 shows the RVE1 cylinder probability distributions for the in-plane orientation angle ϕ in 5° intervals and for the out-of-plane orientation angle θ in intervals of 2°. The corresponding results for RVE2 are shown in Figure 5, where the probability distribution for θ is given in 1° intervals. We note that a certain tendency towards fiber aggregation on preferred orientations can be noticed for both RVEs, being more evident in the case of RVE2. This can be explained through the natural tendency towards fiber aggregation in high fiber volume fraction composites and is a phenomenon also noticed in other studies such as [Duschlbauer et al. 2006]. However, we note that the imposition of the geometry periodicity requirements in the RSA generation algorithm usually tends to exacerbate this tendency.
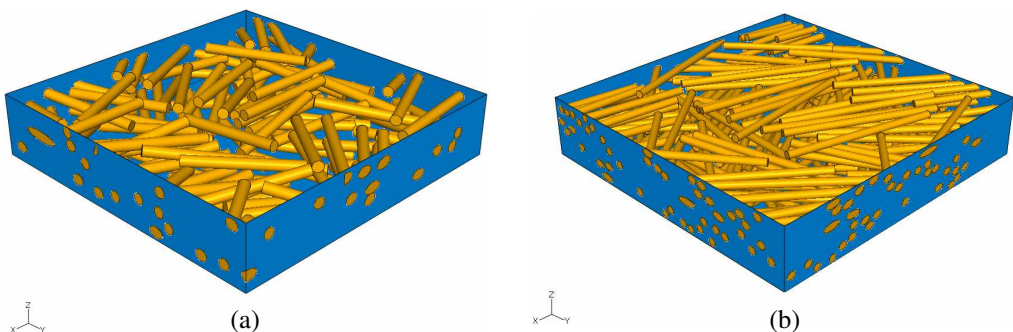

Figure 3. RVE microscale geometries for (a) RVE1 ($v_f = 15\%$, $AR = 10$) and (b) RVE2 ($v_f = 20\%$, $AR = 20$).
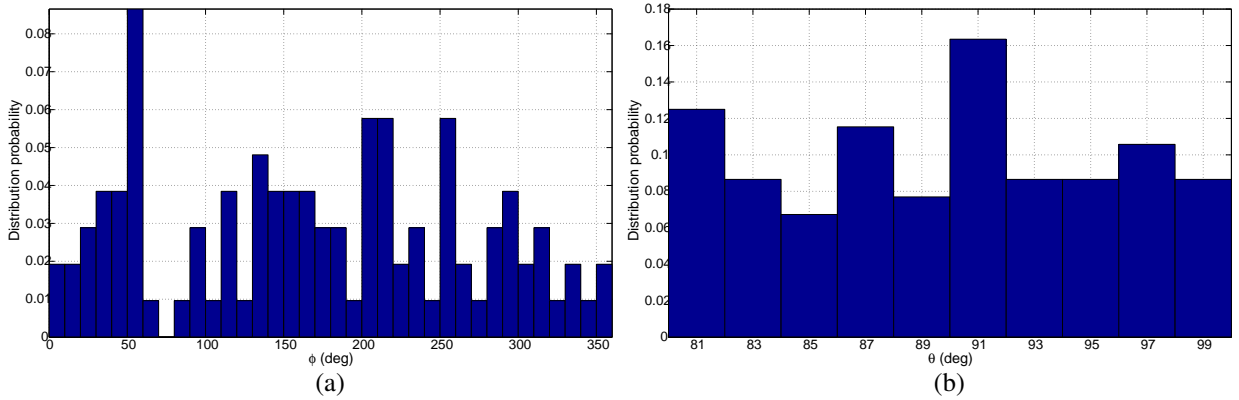
Figure 4. RVE 1: Cylinder orientation distribution (a) in-plane angle ϕ and (b) out-of-plane angle θ.

The two material models considered in this paper will be analyzed using the two generated RVEs and following the approach outlined in the next section.

3. Homogenization scheme

Homogenization approach. The basics of the homogenization procedure are briefly reviewed. In order to determine the properties of an equivalent homogeneous medium that accurately represents, at the macroscopic level (that is, the RVE volume, in this study), the response of the microscopically heterogeneous one, we consider the equivalent macro stress and strain, $\overline{\sigma}$ and $\overline{\epsilon}$, defined as the mean values of the respective fields in the RVE [Sun 2006],

$$\overline{\sigma}_{ij} = \frac{1}{V} \int_V \sigma_{ij}(\boldsymbol{x})\,dV, \qquad \overline{\epsilon}_{ij} = \frac{1}{V} \int_V \epsilon_{ij}(\boldsymbol{x})\,dV, \qquad i, j = 1, 2, 3, \quad \boldsymbol{x} \in V. \tag{1}$$
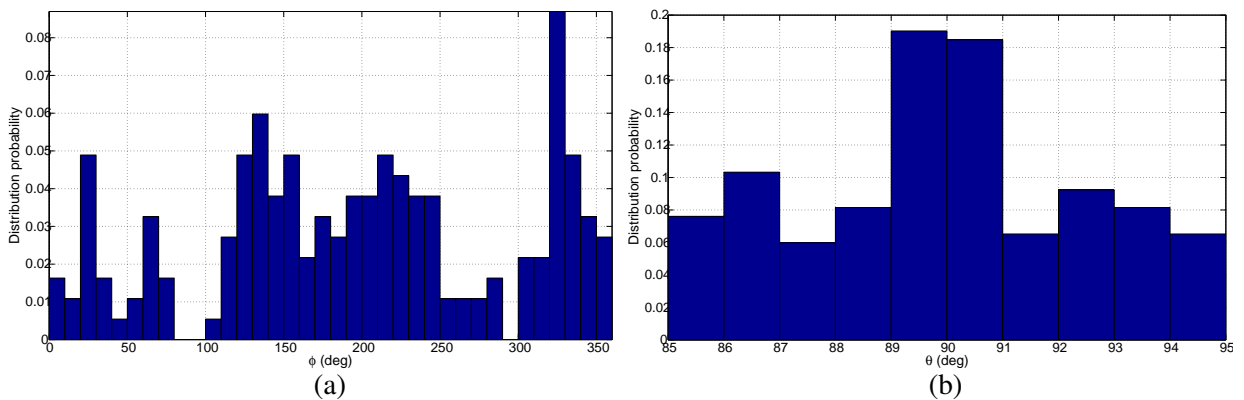

Figure 5. RVE 2: Cylinder orientation distribution (a) in-plane angle ϕ and (b) out-of-plane angle θ.

The effective elastic constants of the homogeneous material can then be defined by the linear constitutive equation,

$$\overline{\sigma}_{ij} = \overline{C}_{ijkl}\overline{\epsilon}_{kl}. \tag{2}$$

We note that the equivalence of the strain energy between the random composite material and the homogeneous one is ensured through the Hill condition [Hill 1971],

$$\frac{1}{2V}\int_V \sigma_{ij}\epsilon_{ij}\,\mathrm{d}V = \frac{1}{2}\overline{\sigma}_{ij}\overline{\epsilon}_{ij}.$$

Boundary conditions. The components of the stiffness tensor of the equivalent homogeneous material, $\overline{C}_{ijkl}$, can be completely determined by solving the state equilibrium solution for six independent loading cases. To this end, we employ kinematic boundary conditions [Sanchez-Palencia and Zaoui 1985; Kanit et al. 2006] that correspond to three pure axial and three pure shear deformations of the RVE. The boundary conditions are specified by imposing a displacement $\boldsymbol{u}$ at a point $\boldsymbol{x}$ on the boundary ∂V, such that $u_i = \epsilon_{ij}^0 x_j$, $\forall \boldsymbol{x} \in \partial V$, where the second order tensor ϵ^0 is independent of $\boldsymbol{x}$ and represents, in effect, a uniformly applied strain. The six loading cases considered here correspond to specifying the nonzero elements of ϵ^0 as follows: $\epsilon_{11}^0 = 10^{-5}$, $\epsilon_{22}^0 = 10^{-5}$, $\epsilon_{33}^0 = 10^{-5}$, $\epsilon_{12}^0 = 10^{-5}$, $\epsilon_{13}^0 = 10^{-5}$ and $\epsilon_{23}^0 = 10^{-5}$.

We note here that kinematic uniform boundary conditions lead to upper estimates of the stiffness tensors [Hazanov and Huet 1994]. It must also be noted that although the boundary conditions imposed in this study are of the uniform strain type, the rationale for the generation of periodic geometries is to provide the means for a future comparison of the numerical results obtained through the imposition of periodic and homogeneous boundary conditions.

Following the simulation of the material response under the load due to the above values of the uniform strain, the average stress and strain in the RVE can be computed using Equation (1). Thus, the use of (2) for each of the loading cases will yield the system of 36 equations from which the values of the stiffness tensor $\boldsymbol{C}$ can be readily determined. The symmetry requirements for the stiffness tensor, which effectively reduce the number of unknowns to 21, are used solely to verify the correctness of the numerical results.

An alternative approach is to directly estimate the average stress in the RVE via an elementary mechanics of materials definition of stress,

$$\overline{\sigma}_{ij} = F_i^j / A, \tag{3}$$

where F_i^j is the i-direction component of the reaction force on the boundary face of area A, which develops in the loading case j (for shear-loading cases $j = 4, 5, 6$, the force is tangential to the face A). Despite its simplicity this approach yields results of comparable accuracy to the actual application of (1), while proving to be significantly faster. The practical aspects of direct FEM implementation and alternative solution approaches employed for validating the direct numerical simulation results are discussed next.

4. RVE numerical simulations

The modeling approach towards solving the six static problems corresponding to the loading cases required for the determination of tensor $\overline{C}$, as well as the alternative approaches used for comparison of

results, namely an orientation averaging approach and the laminated random strand (LRS) method are discussed next.

For the purpose of this work, the fiber and matrix materials for the two composite configurations are considered as E-glass and epoxy, respectively. No particular production composite is analyzed, but the procedure and results are considered to be representative for the material design and selection phase. For E-glass, the Young's modulus and Poisson ratio values used are $E_f = 70$ GPa and $\nu_f = 0.2$, while for the matrix material, $E_m = 3$ GPa and $\nu_m = 0.35$. Furthermore, the E-glass fibers and matrix are isotropic.

4.1. *Finite element modeling.* A three-dimensional solid model is built in the commercial FEA package ABAQUS (version 6.7) by importing the fiber positions and orientation angles. The RVEs are meshed with linear C3D4 4-node tetrahedral elements, with total node counts of approximately 250,000 for RVE1 and 750,000 for RVE2. Node sharing at the fiber-matrix interface is ensured by modeling the RVE as a single part solid. The FEA discretization is restricted primarily by the memory limitations on the available computers. The evaluation of the average stress and strain in the RVEs (see Equation (1)) can be performed approximately using the ABAQUS feature of returning the value of the volume associated with the element integration node. Thus, volume integration of functions can be performed by summing the function values at the integration points, multiplied by the respective elemental volumes. The application of Equation (3) is carried out directly by summation of the nodal reaction forces on the boundary surfaces.

4.2. *Validation approaches.* In order to validate the three-dimensional FEM analysis, two alternative approaches are considered. First, we rely on the orientation averaging scheme of Advani and Tucker [1987] to determine the elastic constants of the random composite based on those of the equivalent material with fully aligned fibers. Second, we employ the LRS method recently proposed by Ionita and Weitsman [2006] as a way of rapidly evaluating the properties of large numbers of fiber arrangements.

Orientation averaging. This approach was validated by Gusev et al. [2002] by an analysis of composites with 15% fiber volume fraction, for different orientation states, which led to the conclusion that orientation averaging offers good engineering predictions. We follow here a similar approach, first constructing RVEs with perfectly aligned, but randomly positioned, cylindrical fibers, and determining by direct FEM analysis their respective stiffness tensor. Next, orientation averaging is performed to obtain an estimate of the equivalent composite with randomly oriented fibers. We will briefly present here the basic concepts of the method.

The orientation of a fiber is fully described by the direction unit vector $\boldsymbol{p}$, that is

$$p_1 = \sin(\theta)\cos(\phi) \qquad p_2 = \sin(\theta)\sin(\phi) \qquad p_3 = \cos(\theta),$$

while the orientation of a whole set of fibers is defined by an infinite series of orientation tensors, $\boldsymbol{a}$. Since the fiber orientation is periodic, meaning a fiber oriented at angles (ϕ, θ) is indistinguishable from one with angles $(\phi + \pi, \pi - \theta)$, due to symmetry considerations, only the even second and fourth order

tensors $\boldsymbol{a}_2$, $\boldsymbol{a}_4$ are relevant. These are defined as

$$a_{ij} = \langle p_i p_j \rangle = \int_0^{2\pi} \int_0^{\pi} p_i p_j \psi(\phi, \theta) \sin(\theta) \, d\theta d\phi,$$

$$a_{ijkl} = \langle p_i p_j p_k p_l \rangle = \int_0^{2\pi} \int_0^{\pi} p_i p_j p_k p_l \psi(\phi, \theta) \sin(\theta) \, d\theta d\phi,$$

where $\psi(\phi, \theta)$ is the probability distribution function characterizing the fiber orientations in the composite. For the cases of mostly in-plane fiber orientations considered in this work, the probability distribution function $\psi(\phi, \theta)$ can be written as

$$\psi(\phi, \theta) = \frac{1}{n} \big[H(\theta - \theta_1) - H(\theta - \theta_2) \big],$$

where $H(\theta)$ denotes the Heaviside step-function and θ_1 and θ_2 are the limits of the interval of variation for the out-of-plane angle θ, that is, $\theta_1 = 80°$, $\theta_2 = 100°$ and $\theta_1 = 85°$, $\theta_2 = 95°$ for RVE1 and RVE2, respectively. The scalar n is a scaling factor such that

$$\int_0^{2\pi} \int_0^{\pi} \psi(\phi, \theta) \sin(\theta) \, d\theta d\phi = 1.$$

As mentioned, due to symmetry considerations, the orientation averaged stiffness tensor $\overline{\boldsymbol{C}}'$ can be completely determined only in terms of the tensors $\boldsymbol{a}_2$ and $\boldsymbol{a}_4$ and the five elastic constants B corresponding to the stiffness tensor of the aligned composite

$$\overline{C}'_{ijkl} = B_1 a_{ijkl} + B_2(a_{ij}\delta_{kl} + a_{kl}\delta_{ij}) + B_3(a_{ik}\delta_{jl} + a_{il}\delta_{jk} + a_{jk}\delta_{il} + a_{jl}\delta_{ik}) + B_4\delta_{ij}\delta_{kl} + B_5(\delta_{ik}\delta_{jl} + \delta_{il}\delta_{jk}),$$

where δ_{ij} denotes the Kronecker delta function and the constants B are given by:

$$B_1 = C_{1111} + C_{2222} - 2C_{1122} - 4C_{1212}, \qquad B_2 = C_{1122} - C_{2233},$$

$$B_3 = C_{1212} + \tfrac{1}{2}(C_{2233} - C_{2222}), \qquad\qquad B_4 = C_{2233},$$

$$B_5 = \tfrac{1}{2}(C_{2222} - C_{2233}).$$

Unidirectional composite analysis. Two alternate unidirectional RVEs, namely RVE1 and RVE2, are generated using the RSA procedure, with constraints $\phi = 0°$ and $\theta = 90°$. RVE1a, which corresponds to the composite configuration with fiber aspect ratio $AR = 10$ and volume fraction $v_f = 15.13\%$, is composed of 128 cylinders enclosed in a cuboid of dimensions $3l_f \times 3l_f \times 0.6l_f$, where l_f is the fiber length. Similarly, for the configuration with fiber aspect ratio $AR = 20$ and volume fraction $v_f = 20\%$, RVE2a has dimensions $1.5l_f \times 1.5l_f \times 0.4l_f$ and includes a total of 132 cylinders. For both RVE1a and RVE2a, a geometry periodicity requirement was imposed on the parallelepiped faces normal to the fiber directions. As in the aforementioned random orientation cases, both RVEs are meshed using 4-node tetrahedron elements, with mesh densities similar to those used for RVE1 and RVE2.

The laminated random strand method. The laminated random strand (LRS) method was recently proposed by Ionita and Weitsman [2006] as an alternative, approximate, approach that allows for the rapid evaluation of a large number of fiber arrangements in a mostly in-plane random fiber orientation. Based

on the composite laminate theory, and approximating the geometry as a series of pseudolayers of randomly oriented strands, the method does not account explicitly for out-of-plane fiber orientations or for strand overlaps. However, it does account for the strand stiffness reduction due to *kinks* at contact points, by statistically determining the average number of contact points and kink size and considering the corresponding average strand stiffness reduction.

The LRS method is, essentially, a windowing-type method. Windowing methods seek to determine lower and upper property estimates as well as bounds through varying the analysis window size [Jiang et al. 2001]. In the LRS method, a rectangular window of size L is selected and in each pseudolayer, N strands are considered such that $\sum_{i=1}^{N} A_i = L^2$, where $A_i = l_i w_i$ is the area covered by the i-th strand in the sampling window, of width w_i and length l_i. Since the elastic properties of the strand, Q_{ij}, as well as the orientation of each strand are known, the transformed properties $\overline{Q}_{ij}$ can be computed in the reference system attached to the sample window. The contribution of each strand stiffness to the total stiffness of the layer in which it is contained is considered proportional to the area ratio $\mu_i = A_i/L^2$. This allows for immediate evaluation of the individual layer stiffnesses and, in turn, the total *random laminate* elastic properties can be readily estimated using the classical laminate theory.

The evaluation of strand elastic properties is done using the well-known Halpin–Tsai equations. Although initially derived for long-fiber composites, and semiempirical in nature, they are based, as pointed out by Hine et al. [2002] on the self-consistent ideas of Hill [1971]. In this work, the parameter ξ in the Halpin–Tsai equations was assigned the widely used value $\xi = 2$, which is known to correctly predict the transverse modulus, while slightly overestimating the Poisson ratio [Hine et al. 2002].

In the present study, a number of 4 pseudolayers was considered for the case of the $v_f = 15.13\%$, $AR = 10$ composite, while 7 pseudolayers were considered for the $v_f = 20\%$, $AR = 20$ material. For the first material, the evaluation is performed for 50 different windows sizes chosen in the interval $[0.5l_f, 7.5l_f]$. The windows are chosen randomly from a $9l_f \times 9l_f \times 0.6l_f$ box, and 50 strand configurations are analyzed for each window size. Similarly, for the second material, sets of 50 strand configurations are analyzed for each of the 50 sampling windows considered for the second material. In this case, the sampling windows are selected randomly from a $9l_f \times 9l_f \times 0.4l_f$ box.

Numerical results. The static analyses corresponding for the loading cases and the homogenization procedure described in Section 3 are performed for RVE1 and RVE2. For RVE1 ($v_f = 15.13\%$, $AR = 10$), the direct three-dimensional numerical analysis yields the stiffness tensor (in contracted notation, in GPa)

$$\overline{C} = \begin{bmatrix} 7.95 & 3.59 & 3.20 & 0 & 0 & 0 \\ 3.59 & 7.41 & 3.16 & 0 & 0 & 0 \\ 3.20 & 3.16 & 5.93 & 0 & 0 & 0 \\ 0 & 0 & 0 & 1.55 & 0 & 0 \\ 0 & 0 & 0 & 0 & 1.55 & 0 \\ 0 & 0 & 0 & 0 & 0 & 2.14 \end{bmatrix}, \tag{4}$$

while for the unidirectional composite characterized by RVE1a,

$$
C = \begin{bmatrix}
10.58 & 3.07 & 2.95 & 0 & 0 & 0 \\
3.07 & 5.94 & 3.10 & 0 & 0 & 0 \\
2.95 & 3.10 & 5.97 & 0 & 0 & 0 \\
0 & 0 & 0 & 1.56 & 0 & 0 \\
0 & 0 & 0 & 0 & 1.56 & 0 \\
0 & 0 & 0 & 0 & 0 & 1.45
\end{bmatrix},
\tag{5}
$$

which, after orientation averaging yields

$$
\overline{C}' = \begin{bmatrix}
7.74 & 3.65 & 3.10 & 0 & 0 & 0 \\
3.65 & 7.54 & 3.10 & 0 & 0 & 0 \\
3.10 & 3.10 & 5.94 & 0 & 0 & 0 \\
0 & 0 & 0 & 1.51 & 0 & 0 \\
0 & 0 & 0 & 0 & 1.52 & 0 \\
0 & 0 & 0 & 0 & 0 & 2.14
\end{bmatrix}.
\tag{6}
$$

We note that in Equations (4)–(6) the null entries correspond to nonzero numerical results. These are, however, three or four orders of magnitude lower than the nonzero ones and, for all practical reasons, can be taken as null. The relative error between the components of the stiffness tensor for the three-dimensional FEM simulation, (4), and the one obtained by orientation averaging, (6), are presented in Figure 6.

We note that the results obtained from RVE1, by direct three-dimensional FEM analysis, indicate that the material approaches a transversely isotropic one, with the axis of symmetry in the 3-direction, as expected. Transverse isotropy requires that $C_{11} = C_{22}$, $C_{44} = C_{55}$, and $C_{66} = (C_{11} - C_{12})/2$. Consequently, the following departures from transverse isotropy are computed,

$$
2\frac{C_{11} - C_{22}}{C_{11} + C_{22}} = 0.7\%, \qquad 2\frac{C_{11} - C_{12} - 2C_{66}}{C_{11} - C_{12} + 2C_{66}} = 8.7\%,
$$
$$
C_{44} = C_{55}, \qquad\qquad 2\frac{C_{13} - C_{23}}{C_{13} + C_{23}} = 1\%,
$$

and are considered small for all practical purposes.

For RVE2 ($v_f = 20\%$, $AR = 20$), the stiffness tensor results are

$$
\overline{C} = \begin{bmatrix}
9.52 & 4.49 & 3.32 & 0 & 0 & 0 \\
4.49 & 10.04 & 3.33 & 0 & 0 & 0 \\
3.32 & 3.33 & 6.41 & 0 & 0 & 0 \\
0 & 0 & 0 & 1.67 & 0 & 0 \\
0 & 0 & 0 & 0 & 1.67 & 0 \\
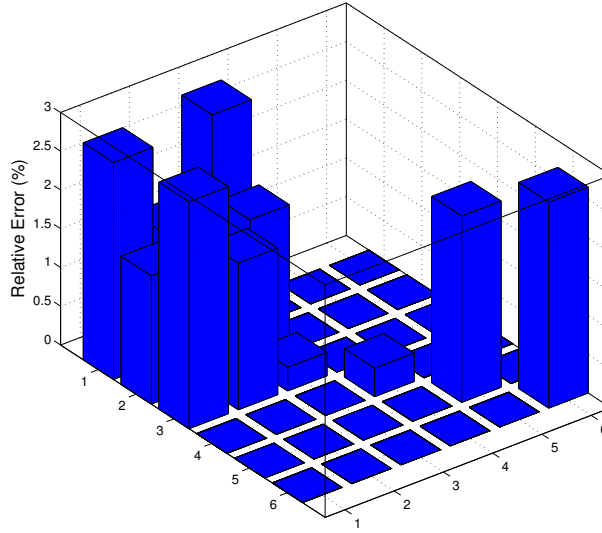0 & 0 & 0 & 0 & 0 & 3.02
\end{bmatrix},
$$

Figure 6. Relative error of stiffness tensor components: RVE1 three-dimensional simulation compared to orientation averaging, $\|\overline{C}_{ij} - \overline{C}'_{ij}\|/\overline{C}'_{ij}$.

while for RVE2a we obtain

$$C = \begin{bmatrix} 15.82 & 3.20 & 3.15 & 0 & 0 & 0 \\ 3.20 & 6.48 & 3.21 & 0 & 0 & 0 \\ 3.15 & 3.21 & 6.60 & 0 & 0 & 0 \\ 0 & 0 & 0 & 1.64 & 0 & 0 \\ 0 & 0 & 0 & 0 & 1.63 & 0 \\ 0 & 0 & 0 & 0 & 0 & 1.47 \end{bmatrix}.$$

The orientation averaged stiffness tensor, for the orientation state characterized by a_2 and a_4 is

$$\overline{C}' = \begin{bmatrix} 9.62 & 4.65 & 3.21 & 0 & 0 & 0 \\ 4.65 & 9.72 & 3.21 & 0 & 0 & 0 \\ 3.21 & 3.21 & 6.48 & 0 & 0 & 0 \\ 0 & 0 & 0 & 1.64 & 0 & 0 \\ 0 & 0 & 0 & 0 & 1.64 & 0 \\ 0 & 0 & 0 & 0 & 0 & 2.99 \end{bmatrix}.$$

The results of the departure from transverse isotropy tests,

$$2\frac{C_{11} - C_{22}}{C_{11} + C_{22}} = 5.34\%, \qquad 2\frac{\frac{1}{2}(C_{11} + C_{22}) - C_{12} - 2C_{66}}{\frac{1}{2}(C_{11} + C_{22}) - C_{12} + 2C_{66}} = 13.29\%,$$

$$C_{44} = C_{55}, \qquad\qquad\qquad\qquad C_{13} = C_{23},$$

display the significant effect of the preferred fiber orientations on the values of C_{11}, C_{22}, and C_{12}. Figure 7 shows the relative error between the components of the stiffness tensor for the two approaches considered.
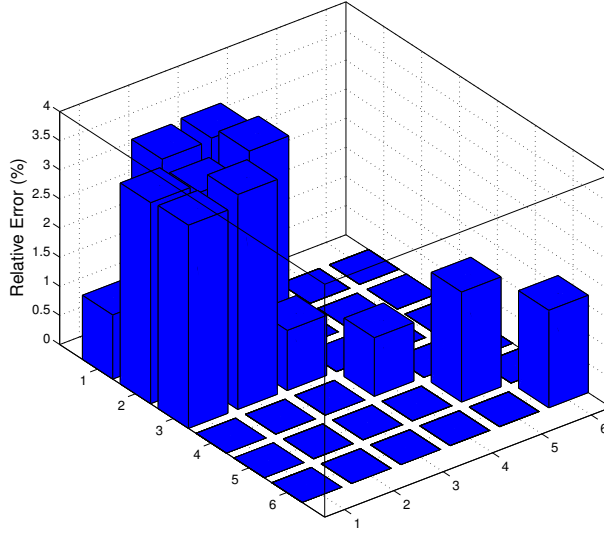
Figure 7. Relative error of stiffness tensor components: RVE2 three-dimensional simulation compared to orientation averaging, $\|\overline{C}_{ij} - \overline{C}'_{ij}\|/\overline{C}'_{ij}$.

5. Automated FEM analysis

With the solution of the RVE geometry and analysis procedure in place, we are interested in the material properties variations that occur locally in a large structure, due to the microscale inhomogeneities — particularly the variation of the fiber volume fraction, caused by fiber aggregation. Consequently, we generate the microgeometry for large panels for each of the materials considered in this study, glass/epoxy $AR = 10$ and $AR = 20$, and we employ a windowing-type analysis. For several sizes of the selected window, a parallelepiped is selected at a random location in the plate. The process is repeated 10 times for each window size and the three-dimensional FEM analysis described earlier is performed for each case. The process, including window selection, meshing and postprocessing of the results, is fully automated and is implemented in ABAQUS via the Python scripting interface. A flowchart of the whole process is illustrated in Figure 8. We note that due to the completely automated nature of the analysis meshing may fail in regions of high geometric complexity, which requires that the model is also automatically checked for complete meshing of all components, as well as for the existence of distorted elements, as shown by the *failed meshing* check block in Figure 8.

In order to analyze the transverse isotropy of the material we consider a measure similar to the one adopted by Ionita and Weitsman [2006]:

$$\Delta = \sqrt{\Delta_1^2 + \Delta_2^2},$$

where

$$\Delta_1 = \frac{2(C_{11} - C_{22})}{C_{11} + C_{22}} \quad \text{and} \quad \Delta_2 = \frac{2(C_{11} - C_{12} - 2C_{66})}{C_{11} + C_{22} + 2C_{66}}.$$
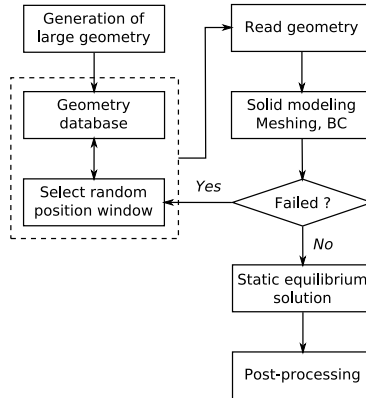
Figure 8. Flowchart of automated three-dimensional FEM windowing analysis.

We also propose a measure of statistical inhomogeneity in the material,

$$\Lambda = \frac{\|C^M - C^K\|}{\|C\|},$$

where M and K, $M \neq K$, denote two nonidentical realizations of a window with the same size, and $\|\cdot\|$ is the matrix 2-norm of the tensor C computed by orientation averaging for an ideally random fiber distribution.

For the first material ($v_f = 15.13\%$), the windowing analysis is performed on a $9l_f \times 9l_f \times 0.6l_f$ box. A number of 20 window sizes L_w are considered in the interval $0.5l_f \leq L \leq 3l_f$ and 10 samples are selected for each value of L_w. The results for the Young's modulus and Poisson ratio are compared to those obtained from LRS in Figures 9 and 10. The departure from isotropy and the statistical inhomogeneity are shown in Figures 11 and 12. It can be noticed that the departure from isotropy becomes smaller with increasing window size, an effect also noticed by Ionita and Weitsman and is explained by the presence of a larger number of fibers in larger samples. An additional explanation lies in the increasing variations in fiber volume fractions, when reducing the sampling window size. This also justifies the larger average values of the Young's modulus for small values of L_w. We note that, while more consistent averages of E may be obtained by increasing the number of sampling windows, at the expense of increased computational time, the evolution of Δ and Λ indicates that, for the materials considered, the use of RVEs of dimensions up to approximately $1.5l_f$ may not be representative.

For the second case analyzed ($v_f = 20\%$), the initial box has dimensions $4l_f \times 4l_f \times 0.4l_f$, limited by the very slow convergence of the generation algorithm at high fiber volume fraction and large dimensions. An analysis similar to the previous one is performed for 10 random samples selected for 16 windows sizes in the interval $[0.5l_f, 2l_f]$. The results for the Young's modulus, Poisson ratio, as well as for the two statistical measures Δ and Λ are shown in Figures 13–16. We note that, unlike in this case of $AR = 10$, while the statistical inhomogeneity Λ reduces with increasing window size, this tendency is not as pronounced for the departure of isotropy Δ. We explain this as an effect of the much smaller domain from which the sampling windows are chosen, which in effect leads to an increased probability of repeatedly including much of the same material subdomains in different analysis windows. We expect
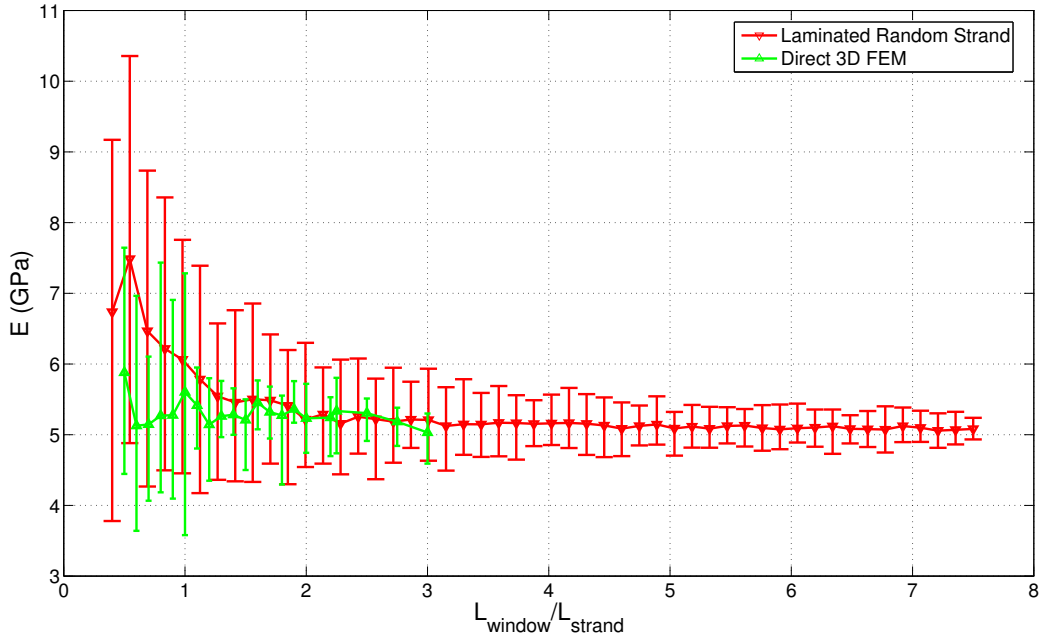
Figure 9. Comparison of predicted equivalent in-plane Young's modulus E versus windows size normalized to strand length, $v_f = 15.13\%$.
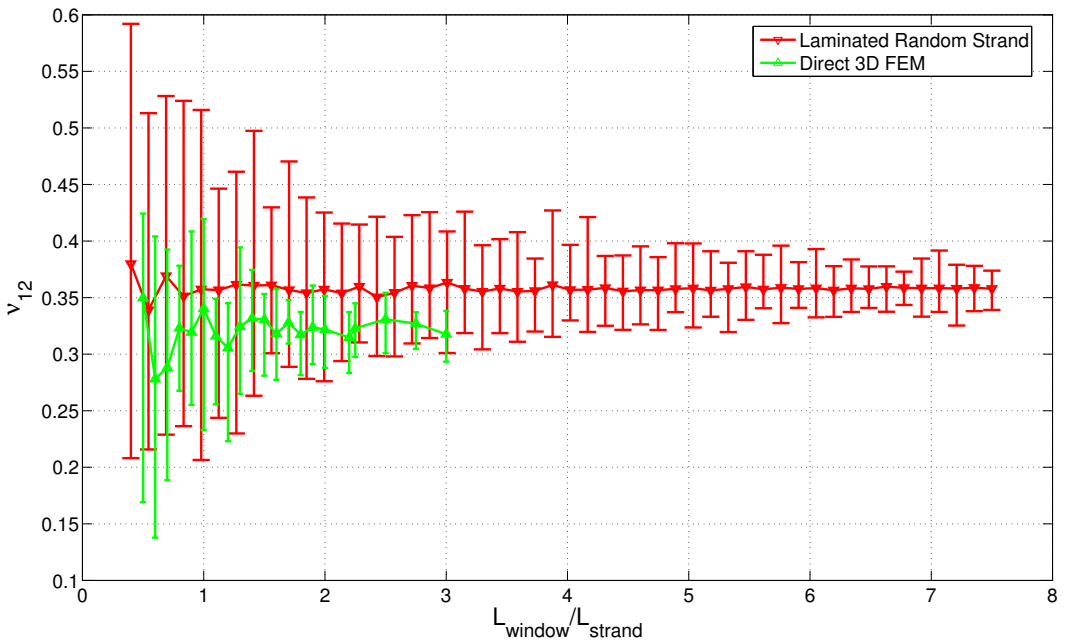

Figure 10. Comparison of predicted in-plane Poisson ratio v_{12} versus window size normalized to strand length, $v_f = 15.13\%$.
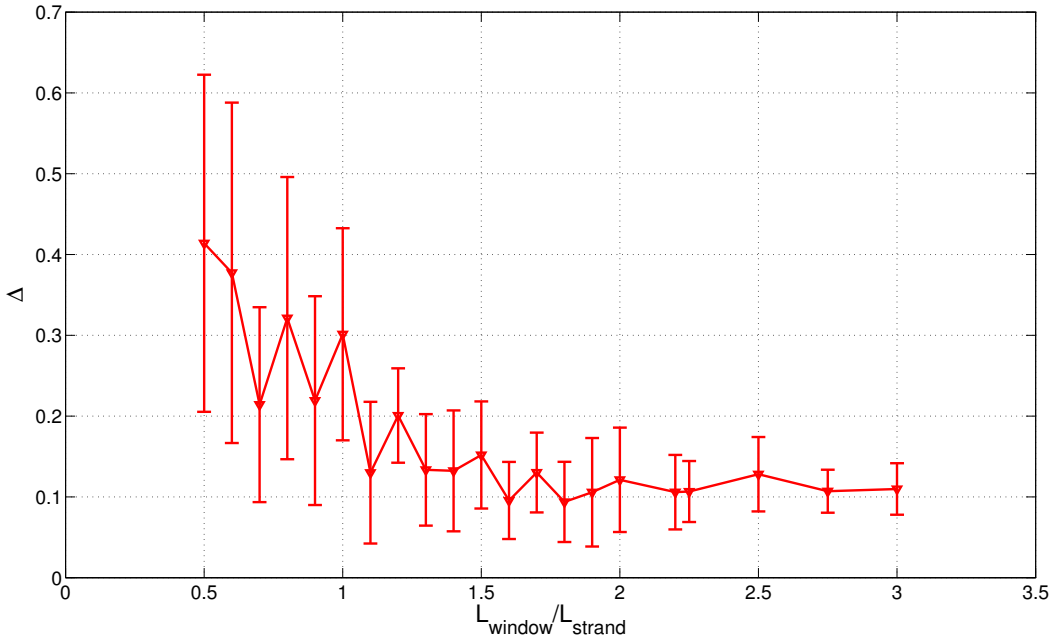
Figure 11. Departure from isotropy Δ versus window size normalized to strand length, $v_f = 15.13\%$.
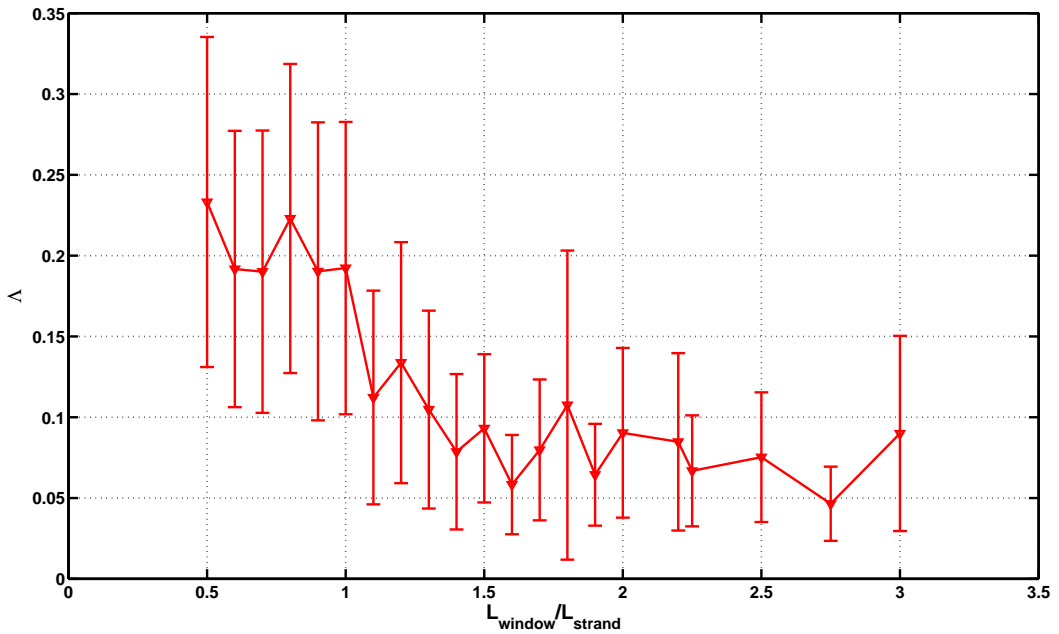

Figure 12. Statistical inhomogeneity Λ versus window size normalized to strand length, $v_f = 15.13\%$.
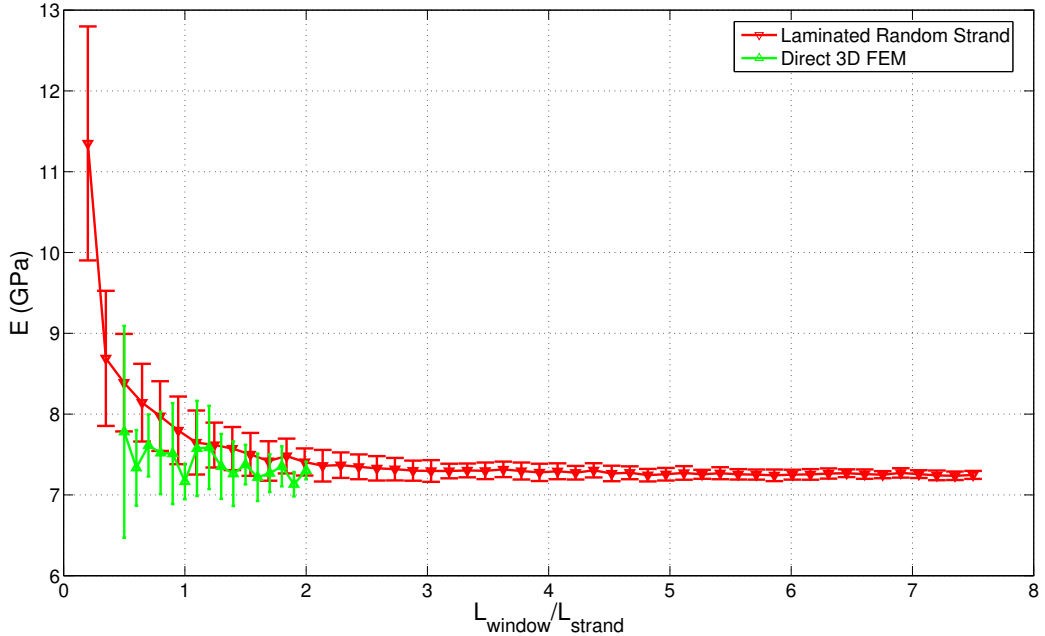
Figure 13. Comparison of predicted equivalent in-plane Young's modulus E versus windows size normalized to strand length, $v_f = 20\%$.

that a steeper reduction can be observed if the dimensions of the initial box are increased, as well as following an increase in the number of samples for each window size. However, we believe the observed behavior of Δ underlines the significant variations in material property that can be observed at the local (micro) level. We also note that the results for the Poisson ratio show, for both LRS and FEM analysis, a remarkable independence with respect to the window size in an average sense. The higher average value in the case of the LRS is due primarily to the choice of the Halpin–Tsai parameter used in computing the strand stiffness.

6. Conclusions

We presented a micromechanical analysis for the determination of the elastic material properties for two types of composite materials with random cylindrical, mostly in-plane oriented short fibers. A random sequential adsorption algorithm was employed for the generation of the microscale geometries and a homogenization technique is employed to determine the equivalent macroscale material properties. The generated RVEs display a tendency towards fiber aggregation on preferred directions due to the geometry periodicity conditions imposed, an effect also noticed in other works. The primary effect is the deviation from the transverse isotropy expected in a composite with an ideally random fiber orientation state. While the RVEs are considered representative for all practical purposes, this emphasizes the difficulty of generating accurate random microscale geometries and the need for more sustained research in this field.
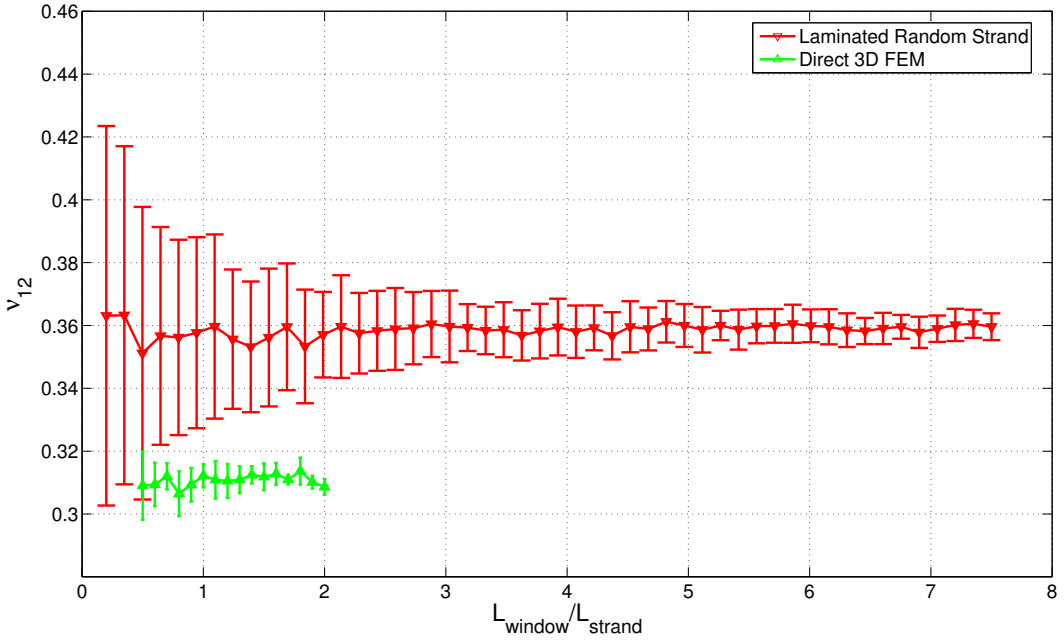
Figure 14. Comparison of predicted in-plane Poisson ratio ν_{12} versus window size normalized to strand length, $v_f = 20\%$.
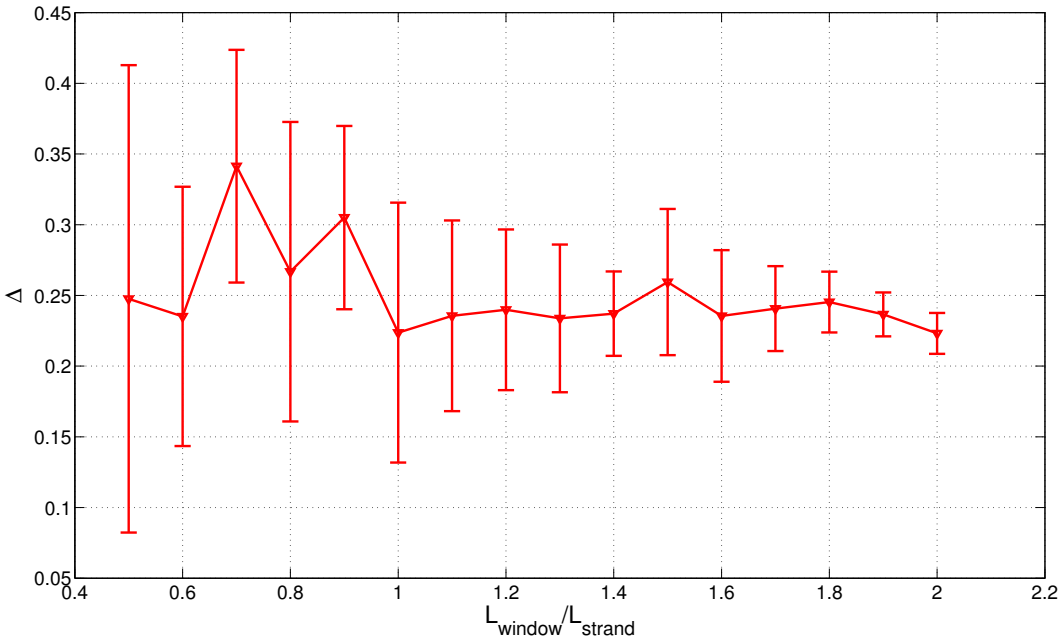

Figure 15. Departure from isotropy Δ versus window size normalized to strand length, $v_f = 20\%$.
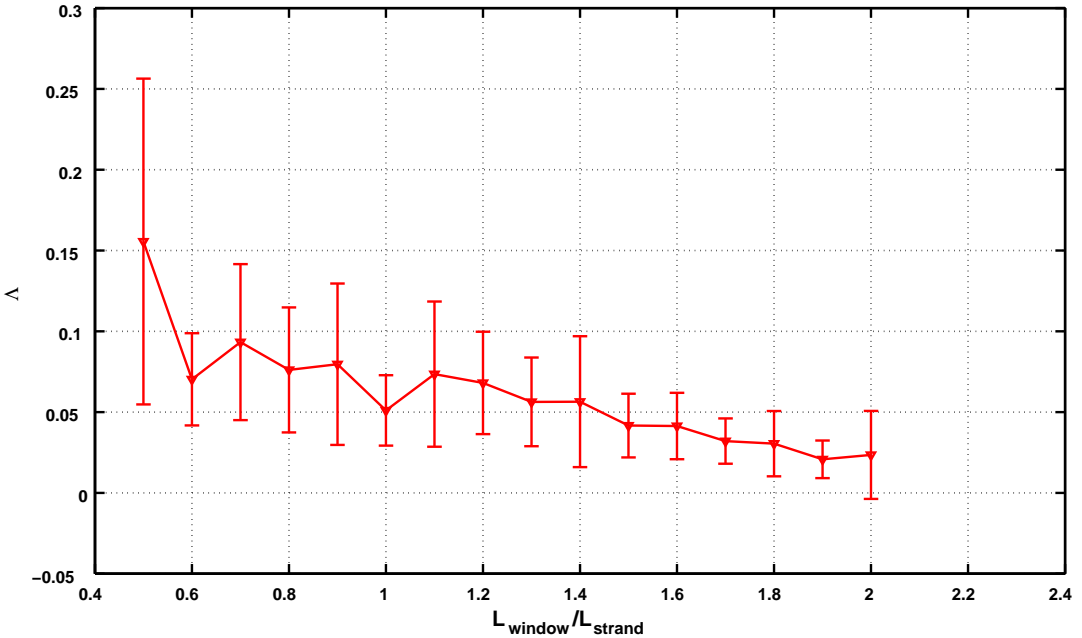
Figure 16. Statistical inhomogeneity Λ versus window size normalized to strand length, $v_f = 20\%$.

Moreover, an evaluation of the material homogeneity for large scale structures was performed. Relatively large plates were generated for the two materials considered and a windowing technique was employed to evaluate the local material properties for different analysis window sizes, using the homogenization technique employed earlier. Although somewhat limited by the reduced number of windows considered, due to the significant computational costs, this analysis indicates that representative volume elements with the side equal to one and a half fiber bundle lengths can be expected to reasonably approximate the homogeneous material properties. We note that the local departure from isotropy can be significant even at higher RVE dimensions, particularly at higher fiber volume fractions, due to the fiber aggregation behavior inherent to the geometry generation algorithm. However, we note that the variations in material properties at the local level, length scales smaller than $1.5l_f$, are significant, as indicated by the values of the departure from isotropy measure Δ and the statistical inhomogeneity Λ. While this can be justified by the already mentioned tendency for preferred fiber orientations, we must also note that no restriction on the *local* fiber volume fraction of the analysis windows has been imposed, leading to variations of the actual volume fraction in the analyzed windows. Thus, the analysis is indicative of an interval of confidence for the local material properties, offering designers an insight on the limits of applicability of the homogenized model and, implicitly, the choice of safety coefficients.

Acknowledgments

References

[Advani and Tucker 1987] S. G. Advani and C. L. Tucker, "The Use of Tensors to Describe and Predict Fiber Orientation in Short Fiber Composites", *Journal of Rheology* **31** (1987), 751–784.

[Benveniste 1987] Y. Benveniste, "A new approach to the application of Mori–Tanaka's theory in composite materials", *Mechanics of Materials* **6**:1 (1987), 147–157.

[Coelho et al. 1997] D. Coelho, J.-F. Thovert, and P. M. Adler, "Geometrical and transport properties of random packings of spheres and aspherical particles", *Physical Review E* **55**:2 (1997), 1959–1978.

[Dahl et al. 2005] J. S. Dahl, G. Smith, D. Houston, and L. Berger, "The influence of fiber tow size on the performance of chopped carbon fiber reinforced composites", *Materials and processing technologies for revolutionary applications, 37th ISTC,Washington* (2005).

[Duschlbauer et al. 2006] D. Duschlbauer, H. J. Böhm, and H. E. Pettermann, "Computational Simulation of Composites Reinforced by Planar Random Fibers: Homogenization and Localization by Unit Cell and Mean Field Approaches", *Journal of Composite Materials* **40**:24 (2006), 2217–2234.

[Eberly 2001] D. Eberly, "Intersection of Cylinders", http://www.geometrictools.com, 2001.

[Eshelby 1957] J. D. Eshelby, "The determination of the elastic field of an ellipsoidal inclusion, and related problems", *Proceedings of the Royal Society of London. Series A* **241**:1226 (1957), 376–396.

[Gusev et al. 2002] A. Gusev, M. Heggli, H. Lusti, and P. Hine, "Orientation Averaging for Stiffness and Thermal Expansion of Short Fiber Composites", *Advanced Engineering Materials* **4**:12 (2002), 931–933.

[Hazanov and Huet 1994] S. Hazanov and C. Huet, "Order relationships for boundary conditions effect in heterogeneous bodies smaller than the representative volume", *Journal of the Mechanics and Physics of Solids* **42**:12 (1994), 1995–2011.

[Hill 1971] R. Hill, "Elastic properties of reinforced solids: some theoretical principles", *Journal of the Mechanics and Physics of Solids* **11**:5 (1971), 357–372.

[Hine et al. 2002] P. J. Hine, H. R. Lusti, and A. A. Gusev, "Numerical simulation of the effects of volume fraction, aspect ratio and fibre length distribution on the elastic and thermoelastic properties of short fibre composites", *Composites science and technology* **62**:10-11 (2002), 1445–1453.

[Ionita and Weitsman 2006] A. Ionita and W. J. Weitsman, "On the mechanical response of randomly reinforced chopped-fibers composites: Data and model", *Composites Science and Technology* **66** (2006), 2566–2579.

[Jiang et al. 2001] M. Jiang, K. Alzebdeh, I. Jasiuk, and M. Ostoja-Starzewski, "Scale and boundary conditions effects in elastic properties of random composites", *Acta Mechanica* **vol.148** (2001), 63–78.

[Kanit et al. 2006] T. Kanit, F. N'Guyen, S. Forest, D. Jeulin, M. Reed, and S. Singleton, "Apparent and effective physical properties of heterogeneous materials: Representativity of samples of two materials from food industry", *Computer Methods in Applied Mechanics and Engineering* **195**:33-36 (July 2006), 3960–3982.

[Kari et al. 2007] S. Kari, H. Berger, and U. Gabbert, "Numerical evaluation of effective material properties of randomly distributed short cylindrical fibre composites", *Computational Materials Science* **39** (2007), 198–204.

[Mori and Tanaka 1973] T. Mori and K. Tanaka, "Average stress in matrix and average elastic energy of materials with misfitting inclusions", *Acta Metallurgica* **21** (1973), 571–574.

[Pan et al. 2007] Y. Pan, A. A. Pelegri, and L. Iorga, "Analysis of 3D random chopped fiber reinforced composite using the finite element method", *Accepted for publication in Computational Materials Science* (2007).

[Sanchez-Palencia and Zaoui 1985] E. Sanchez-Palencia and A. Zaoui (editors), *Homogenization techniques for composite media : Lectures delivered at the* CISM *International Center for Mechanical Science*, Lecture Notes in Physics, Springer-Verlag, 1985.

[Sun 2006] C. Sun, "Mechanics of Composite Materials and Laminates - Lecture Notes", 2006. unpublished.

[Williams and Philipse 2003] S. Williams and A. Philipse, "Random packings of spheres and spherocylinders simulated by mechanical contraction", *Physical Review E* **67**:5 (May 2003), 051301.

LUCIAN IORGA: liorga@rci.rutgers.edu
Mechanical and Aerospace Engineering, School of Engineering, Rutgers University, 98 Brett Road, Piscataway, NJ 08854-8058, United States

YI PAN: yipan@eden.rutgers.edu
Mechanical and Aerospace Engineering, School of Engineering, Rutgers University, 98 Brett Road, Piscataway, NJ 08854-8058, United States

ASSIMINA PELEGRI: pelegri@jove.rutgers.edu
Mechanical and Aerospace Engineering, School of Engineering, Rutgers University, 98 Brett Road, Piscataway, NJ 08854-8058, United States